AGU PUBLICATIONS

JGR

Journal of Geophysical Research: Planets

RESEARCH ARTICLE
10.1002/2014JE004623

Special Section:
Results from the first 360 Sols of the Mars Science Laboratory Mission: Bradbury Landing through Yellowknife Bay

Key Points:
- Raised ridges are early diagenetic cement-filled cracks in Sheepbed mudstone
- Cracks are subaqueous shrinkage cracks likely formed by subsurface gas
- Isopachous cement fills indicate series of pore fluid chemistries

Correspondence to:
K. L. Siebach,
ksiebach@caltech.edu

Citation:
Siebach, K. L., J. P. Grotzinger, L. C. Kah, K. M. Stack, M. Malin, R. Léveillé, and D. Y. Sumner (2014), Subaqueous shrinkage cracks in the Sheepbed mudstone: Implications for early fluid diagenesis, Gale crater, Mars, *J. Geophys. Res. Planets*, *119*, 1597–1613, doi:10.1002/2014JE004623.

Received 5 FEB 2014
Accepted 22 JUN 2014
Accepted article online 27 JUN 2014
Published online 17 JUL 2014

Subaqueous shrinkage cracks in the Sheepbed mudstone: Implications for early fluid diagenesis, Gale crater, Mars

K. L. Siebach[1], J. P. Grotzinger[1], L. C. Kah[2], K. M. Stack[1], M. Malin[3], R. Léveillé[4,5], and D. Y. Sumner[6]

[1]Department of Geological and Planetary Sciences, California Institute of Technology, Pasadena, California, USA, [2]Department of Earth and Planetary Sciences, University of Tennessee, Knoxville, Knoxville, Tennessee, USA, [3]Malin Space Science Systems, San Diego, California, USA, [4]Canadian Space Agency, St. Hubert, Quebec, Canada, [5]Department of Earth and Planetary Science, McGill University, Montreal, Quebec, Canada, [6]Department of Earth and Planetary Sciences, University of California, Davis, California, USA

Abstract The Sheepbed mudstone, Yellowknife Bay formation, Gale crater, represents an ancient lakebed now exhumed and exposed on the Martian surface. The mudstone has four diagenetic textures, including a suite of early diagenetic nodules, hollow nodules, and raised ridges and later diagenetic light-toned veins that crosscut those features. In this study, we describe the distribution and characteristics of the raised ridges, a network of short spindle-shaped cracks that crosscut bedding, do not form polygonal networks, and contain two to four layers of isopachous, erosion-resistant cement. The cracks have a clustered distribution within the Sheepbed member and transition laterally into concentrations of nodules and hollow nodules, suggesting that these features formed penecontemporaneously. Because of the erosion-resistant nature of the crack fills, their three-dimensional structure can be observed. Cracks that transition from subvertical to subhorizontal orientations suggest that the cracks formed within the sediment rather than at the surface. This observation and comparison to terrestrial analogs indicate that these are syneresis cracks—cracks that formed subaqueously. Syneresis cracks form by salinity changes that cause sediment contraction, mechanical shaking of sediment, or gas production within the sediment. Examination of diagenetic features within the Sheepbed mudstone favors a gas production mechanism, which has been shown to create a variety of diagenetic morphologies comparable to the raised ridges and hollow nodules. The crack morphology and the isopachous, layered cement fill show that the cracks were filled in the phreatic zone and that the Sheepbed mudstone remained fluid saturated after deposition and through early burial and lithification.

1. Introduction

Whereas Mars was once considered to be a mostly volcanic planet, the last 10 years of exploration have shown that there are a significant number of sedimentary deposits on Mars and that these rocks record a complex history of water-rock interaction [*McLennan and Grotzinger*, 2008; *Grotzinger and Milliken*, 2012]. Orbital-based observations have shown that these rocks form in a range of depositional environments and show a wide variety of spectral signatures [e.g., *Ehlmann et al.*, 2008; *McLennan*, 2012]. More detailed investigations into sedimentary clast origins, depositional textures, rock lithification, and later rock modifications must be completed at the rover scale. Diagenesis, in particular, includes all processes that occur after initial sediment deposition and prior to weathering and erosion of an exhumed rock, including the lithification of sediments into rock. Investigation into the diagenetic stages that sediments have undergone helps constrain the duration, continuity, and chemistry of different stages of water-rock interaction. The diagenesis of sediments usually encompasses loss of porosity due to grain reorganization, compaction, and cementation of the rock and may also include authigenic mineral precipitation, void formation, and sediment deformation [*Worden and Burley*, 2003]. Later diagenetic affects may also include events related to creation of new pore networks, often associated with fracturing and subsequent fluid migration events [*Long et al.*, 1996]. Detailed studies of mineralogy, chemical variability, and textural features can aid in reconstruction of these diagenetic events. Ultimately, understanding diagenetic histories can provide critical constraints on the reconstruction of ancient depositional environments and the chemical evolution of sedimentary pore fluids.

The effects of sediment diagnesis have been observed on Mars at both rover [*Clark et al.*, 2005; *McLennan et al.*, 2005] and orbiter scales [*Okubo and McEwen*, 2007; *Ehlmann et al.*, 2011; *Siebach and Grotzinger*, 2013]

and have been attributed to the circulation of liquid water through pore networks. In some cases, these observations provide plausible constraints on the volume of water required to form diagenetic signals [e.g., *McLennan et al*., 2005; *Siebach and Grotzinger*, 2013]. At present, most of the diagenetic processes observed by landed missions on Mars, like the sulfate cementation at Meridiani Planum, have pointed to acidic, highly saline groundwaters with low water activity [*Grotzinger et al*., 2005; *McLennan et al*., 2005; *Knoll and Grotzinger*, 2006; *Tosca et al*., 2008]; however, these compositions may be inherently biased due to the small number of landed missions. More recent findings from the Mars Exploration Rover and Mars Science Laboratory (MSL) missions have shown that more neutral-pH environments, with lower salinity and elevated water activity, were also present on early Mars [*Arvidson et al*., 2014; *McLennan et al*., 2014; *Vaniman et al*., 2014] and that these were potentially habitable environments that could have been suitable for chemolithoautotrophic microbes [*Grotzinger et al*., 2014].

Since landing in August 2012, the *Curiosity* rover has identified multiple types of sedimentary rock, ranging from conglomerate [*Williams et al*., 2013] to sandstone and fine-grained mudstone, each of which provides evidence for diagenesis [*Grotzinger et al*., 2014]. The Sheepbed mudstone, interpreted to have been deposited in an ancient freshwater lake, has undergone extensive study with the full range of analytical instruments on the *Curiosity* rover [*Grotzinger et al*., 2014]. The Sheepbed mudstone is uniformly fine-grained ($<$63 μm grain sizes), composed of $>$15% authigenetic clay minerals [*McLennan et al*., 2014; *Vaniman et al*., 2014], and contains at least four distinct diagenetic textures: nodules (spheroidal protrusions with no discernable internal structure), hollow nodules (spheroidal protrusions showing a central void), raised ridges, and a later generation of gypsiferous, mineralized veins [*Grotzinger et al*., 2014; M. Nachon et al., Calcium sulfate veins characterized by the ChemCam instrument at Gale crater, Mars, submitted to *Journal of Geophysical Research*, 2014; *Stack et al*., 2014]. Collectively, these features record long-term exposure to water and reveal a once-habitable environment in Yellowknife Bay, Mars [*Grotzinger et al*., 2014]. Here we investigate the importance of the raised ridge features and use their characteristics to show that the Sheepbed mudstone was most likely deposited subaqueously and had fluid-saturated pore spaces throughout early lithification and cementation of the mudstone.

2. Geologic Context

After landing at Bradbury Rise (4.589°N, 137.441°E), Gale crater, Mars, the *Curiosity* rover traversed 445 m west to the Glenelg region [*Parker et al*., 2013; *Grotzinger et al*., 2014]. This region represents the conjunction of three units, defined in orbital images based on geomorphic and thermal inertia attributes, which are located at the distal end of an alluvial fan system [*Grotzinger et al*., 2014]. One of the units that *Curiosity* investigated in detail was the bright, fractured (BF) unit, characterized by relatively high thermal inertia, exposed light-toned bedrock, and ubiquitous decimeter-scale fractures. An approximately 5 m thick exposure of stratigraphic section of the BF unit occurs at Glenelg and has been described as the Yellowknife Bay formation [*Grotzinger et al*., 2014]. In ascending order the latter is subdivided into the Sheepbed, Gillespie Lake, and Glenelg members (Figure 1). The uppermost Glenelg member consists of fine- to coarse-grained, locally cross-stratified, basaltic sandstone that is interpreted to reflect fluvial to eolian deposition [*Grotzinger et al*., 2014]. The Gillespie Lake member, also interpreted as a fluvial deposit, consists of a medium-grained sandstone of basaltic composition. Underlying these two more coarsely grained deposits rests the Sheepbed member, a mudstone, also of basaltic composition, that is interpreted to have been deposited in a lacustrine setting [*Grotzinger et al*., 2014]. The contact of the Sheepbed member with the overlying Gillespie Lake member is sharp and traceable in orbital imagery.

The stratigraphically lowest unit in the Glenelg region, the Sheepbed member, is exposed in the floor of Yellowknife Bay. Based on *Curiosity*'s observations, it extends across at least the ~60 m traversed within Yellowknife Bay. Given that it can be traced from orbit, and likely closely coincides with the BF unit, the Sheepbed member is inferred to extend laterally at least several hundred more meters to the east and north and is possibly laterally continuous for hundreds of meters or kilometers beneath the overlying units of the Yellowknife Bay formation [*Grotzinger et al*., 2014]. The Sheepbed member is the best characterized member of the Yellowknife Bay formation because two drilled samples, John Klein and Cumberland, were acquired from this member and analyzed by *Curiosity*'s full analytical instrument suite, including a mass spectrometer

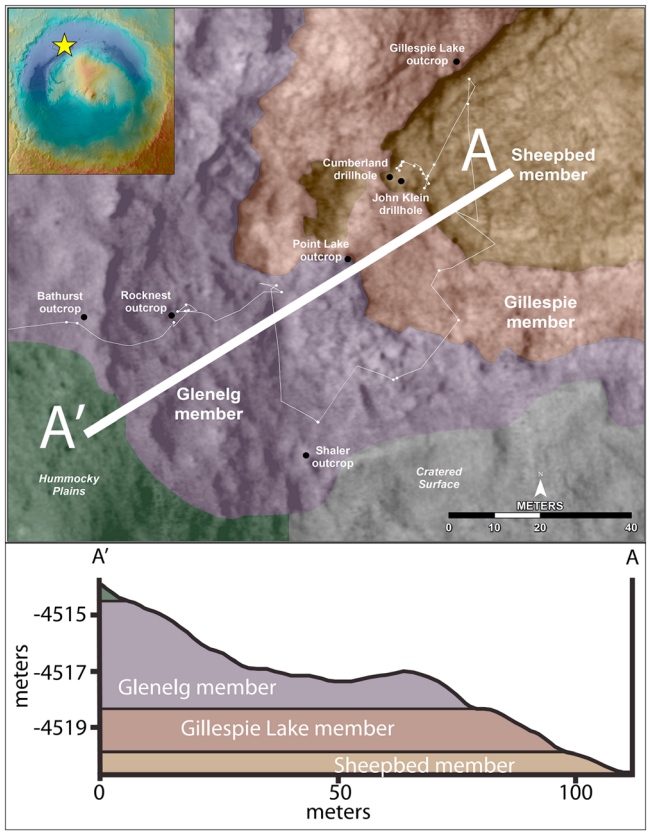

Figure 1. Geologic map of Yellowknife Bay, after *Grotzinger et al.* [2014]. Upper left inset shows Gale crater, 155 km across, with star at Yellowknife Bay location. Lower portion shows members of the Yellowknife Bay formation projected into a HiRISE-extracted elevation profile.

and X-ray diffraction (XRD) instrument [*Ming et al.*, 2014; *Vaniman et al.*, 2014]. In addition, a suite of Alpha-Particle X-Ray Spectrometer (APXS) measurements were collected within the unit [*Grotzinger et al.*, 2014; *McLennan et al.*, 2014], and numerous ChemCam laser-induced breakdown spectroscopy analyses were obtained to help characterize the site (Nachon et al., submitted manuscript, 2014; R. J. Léveillé et al., Chemistry of fracture-filling raised ridges in Yellowknife Bay, Gale crater: window into past aqueous activity and habitability on Mars, submitted to *Journal of Geophysical Research*, 2014). *Curiosity*'s investigation demonstrated that the Sheepbed member is uniformly fine grained, with a near-typical basalt composition, and contains nearly 20% saponitic smectite clay minerals [*Grotzinger et al.*, 2014; *McLennan et al.*, 2014; *Vaniman et al.*, 2014]. The smectite clay, identified by the XRD analysis, was inferred to be authigenic based on the distributed APXS measurements, which showed that the rock chemically matches slightly alkaline average Martian crustal basalt in all of the samples, suggesting isochemical weathering [*McLennan et al.*, 2014]. Mudstones are generally deposited in low-energy, standing water environments, and the Sheepbed unit, in particular, has been interpreted to have been deposited in a lake that formed at the distal limit of an alluvial fan [*Grotzinger et al.*, 2014].

Diagenetic textures representing at least two distinct postdepositional fluid environments are present in the Sheepbed mudstone. These include nodules, hollow nodules, raised ridges, and light-toned, crosscutting, calcium sulfate-rich light-toned veins (Figure 2) [*Grotzinger et al.*, 2014]. The nodules and hollow nodules are millimeter-scale resistant spherical protrusions (sometimes with a less-resistant or hollow center) that are densely clustered in some locations [*Stack et al.*, 2014] and pass laterally into concentrations of raised ridges. The light-toned veins weather flush with the surrounding rock and crosscut the raised ridges, nodules, and hollow nodules (Figure 2).

3. Methods

Raised ridges—mineralized cracks, only a few millimeters in width, which are distributed within the Sheepbed member—were mapped over 27 m^2 of the exposed surface of the Sheepbed unit using ArcGIS software and images available through the NASA Planetary Data System. Context for this mapping was derived from High Resolution Imaging Science Experiment (HiRISE) images (25 cm/pixel) [*McEwen et al.*, 2007] and orthorectified MSL Navigation Camera (Navcam) imagery [*Maki et al.*, 2012], which have been localized along the rover's traverse by the MSL science team localization scientists based on a controlled photomosaic of sequentially higher resolution data sets tied to the Mars Orbital Laser Altimetry global base map [*Parker et al.*, 2013]. HiRISE imagery was used as a basemap for stratigraphic analysis, and rover-based Navcam imagery was used to create contours and localize ChemCam and drill targets. Neither of these image sets, however, provides adequate resolution to map the raised ridge features.

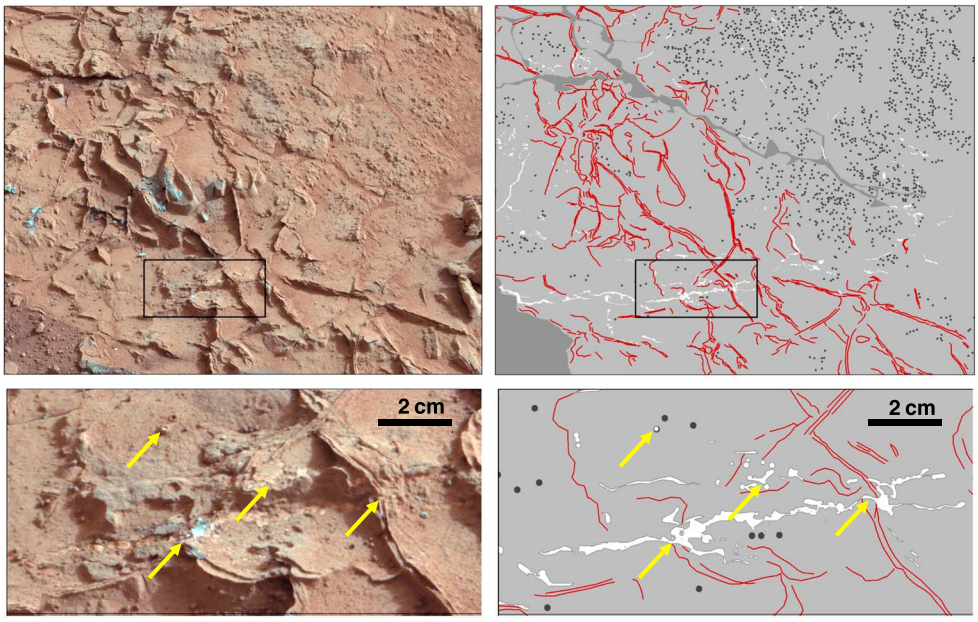

Figure 2. Portions of Mastcam M-100 mosaic (mcam00885, sol 164), with accompanying sketches, showing relationships between diagenetic textures in the Sheepbed unit. Inset box is approximately 13 cm × 6 cm; 2 cm scale bar in inset. Red lines are erosion-resistant cements that compose the raised ridges, dark grey circles are nodules and hollow nodules, white fill shows light-toned veins visible at the surface (many are dust covered), and dark grey depicts dust-covered regions of the mudstone. Yellow arrows in inset highlight crosscutting relationship showing that the light-toned veins are a later texture that cut through the raised ridges and hollow nodules, sometimes even filling previously hollow nodules.

The *Curiosity* Mast Camera (Mastcam) imagery proved to be the best available imagery to map the submillimeter-scale raised ridge features over a large spatial area (~27 m^2). The Mastcam consists of two mast-mounted cameras that sit approximately 2.1 m above the surface. The right Mastcam (M-100) has a 100 mm focal length, f/10 lens, with a 6.3° × 5.1° field of view (FOV), and the left Mastcam (M-34) has a 34 mm focal length, f/8 lens, with an 18.4° × 15° FOV. The two cameras are separated by a 24.5 cm stereo baseline [*Malin et al*., 2010; *Bell et al*., 2013]. Image mosaics taken with the M-100 camera are preferable for mapping the raised ridge features because of their inherent higher image resolution; even for surfaces 5 m away from the rover, the M-100 camera provides a resolution of 0.37 mm/pixel, whereas the M-34 has a resolution of 1.1 mm/pixel. However, because the images are not taken vertically, but at a variable angle, raw M-100 imagery is necessarily distorted relative to the actual topography of the raised ridges. Thus, where available, stereo imagery was used to create orthorectified Mastcam mosaics using the Ames stereo pipeline [*Moratto et al*., 2010], which was adapted by Malin Space Science Systems to work with the different resolutions of the two Mastcams (see Appendix A). Orthorectified Mastcam mosaics were able to be more accurately correlated to the Navcam-based map and permitted raised ridges to be traced over the key areas of the Sheepbed member with reference to the vertically projected M-100 mosaics when needed for higher resolution (or to correct distortions introduced in the image orthorectification process).

In addition to the large-scale mapping, a Mastcam mosaic, mcam00885, taken on sol 164, was selected for fine-detail mapping of the individual cement layers in the raised ridges and the relationship of the raised ridges to the other diagenetic features in the Sheepbed member. This mapping was also accomplished in ArcGIS, but in this case, because it was critical that the features not be distorted, the rover-perspective white-balanced mosaic was used and the average scene pixel scale (0.206 μm/pixel) was used for measurements of the length and width of 300 individual ridges and cements.

4. Observations

Raised ridges within the Sheepbed mudstone occur as cracks in the mudstone filled with multiple layers of cement. The outermost layer of cement fill is resistant to erosion, resulting in curvilinear ridges that outline the original crack shape, stand above the host rock, and give these features the name "raised ridges." Interior

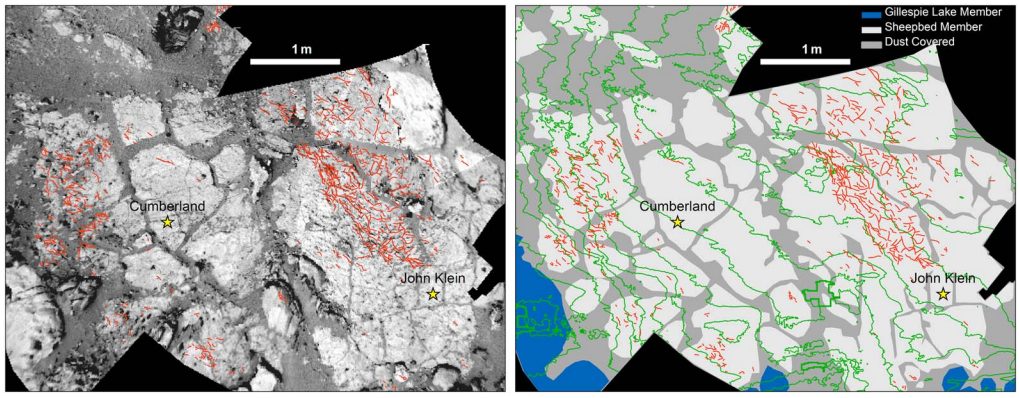

Figure 3. Vertically projected map, showing the distribution of raised ridges (red lines) throughout the mapped area. (left) The ridges are shown on a mosaic of rover navigation camera images. (right) The same mosaic is mapped to show Sheepbed member exposures in light grey, Gillespie Lake member in blue, and dust-covered regions in dark grey. Five centimeter contours based on the Navcam mosaic from sol 159 are shown in green. The John Klein and Cumberland drill sites are identified with yellow stars. Ridges show a clustered distribution both horizontally (within contours) and vertically (across contours) and therefore are not confined by bedding planes.

cement layers are usually less resistant, although in some cracks multiple layers of resistant cements are visible (e.g., Figure 2). The redundancy in the term raised ridges is meant to emphasize the height of the ridges relative to their width.

Raised ridges were mapped comprehensively in the vicinity of the John Klein and Cumberland drill sites where near-rover orthorectified overhead imagery was available (Figure 3). Bedding is rarely visible in this local area, but it is assumed to be near horizontal and to follow contour lines based on an observed near-horizontal contact with the Gillespie Lake member [*Grotzinger et al*., 2014]. The most obvious feature of the raised ridges at the meter scale is their clustered distribution (Figure 3). Laterally, a few concentrated clusters of raised ridges are visible, each region measuring tens of centimeters in diameter. Individual ridge networks do not continue laterally within the same contour interval (i.e., within the same stratigraphic horizon) but transition into either relatively featureless mudstone or areas of concentrated nodules and hollow nodules (e.g., Figure 2; *Stack et al*., 2014). Additionally, both individual ridges and ridge networks crosscut topographic contours (Figure 3). Some raised ridges are not localized within the larger clusters but scattered both laterally and vertically through the mudstone. There is not a consistent preferred crack orientation (Figure 3). At least two ridge clusters (one in Figure 3 and another called the "Rowatt" cluster, Figure A2) occur immediately beneath the Sheepbed-Gillespie Lake contact, and in one location a single raised ridge appears to crosscut the Sheepbed-Gillespie Lake contact.

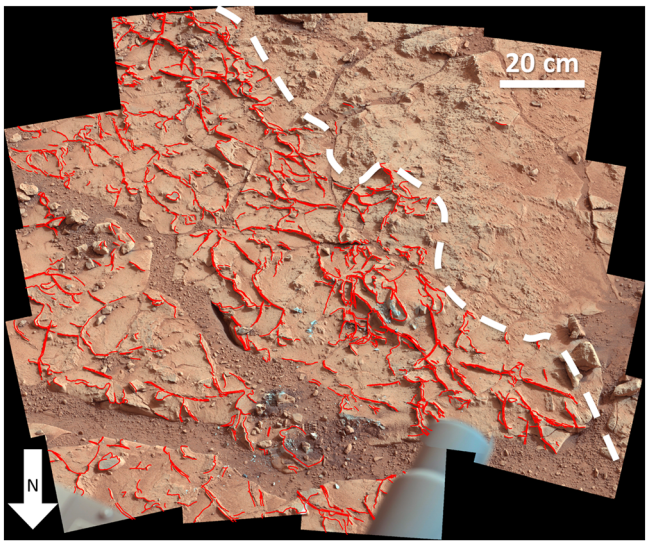

Figure 4. Detailed map of individual raised ridges (red) traced on Mastcam mosaic mcam00885 from sol 164. White dashed line highlights lateral shift in texture from (left) raised ridges to (right) nodules plus hollow nodules.

Detailed mapping of lengths, widths, and shapes of raised ridges within the dense cluster of ridges near the John Klein drill site (Figure 4) shows the characteristics of the crack morphologies and details of fill patterns (e.g., Figure 5). Erosionally resistant infill permits clear identification of the original crack morphology as represented by current ridge morphology. The raised ridges average 6.8 cm in length but can reach

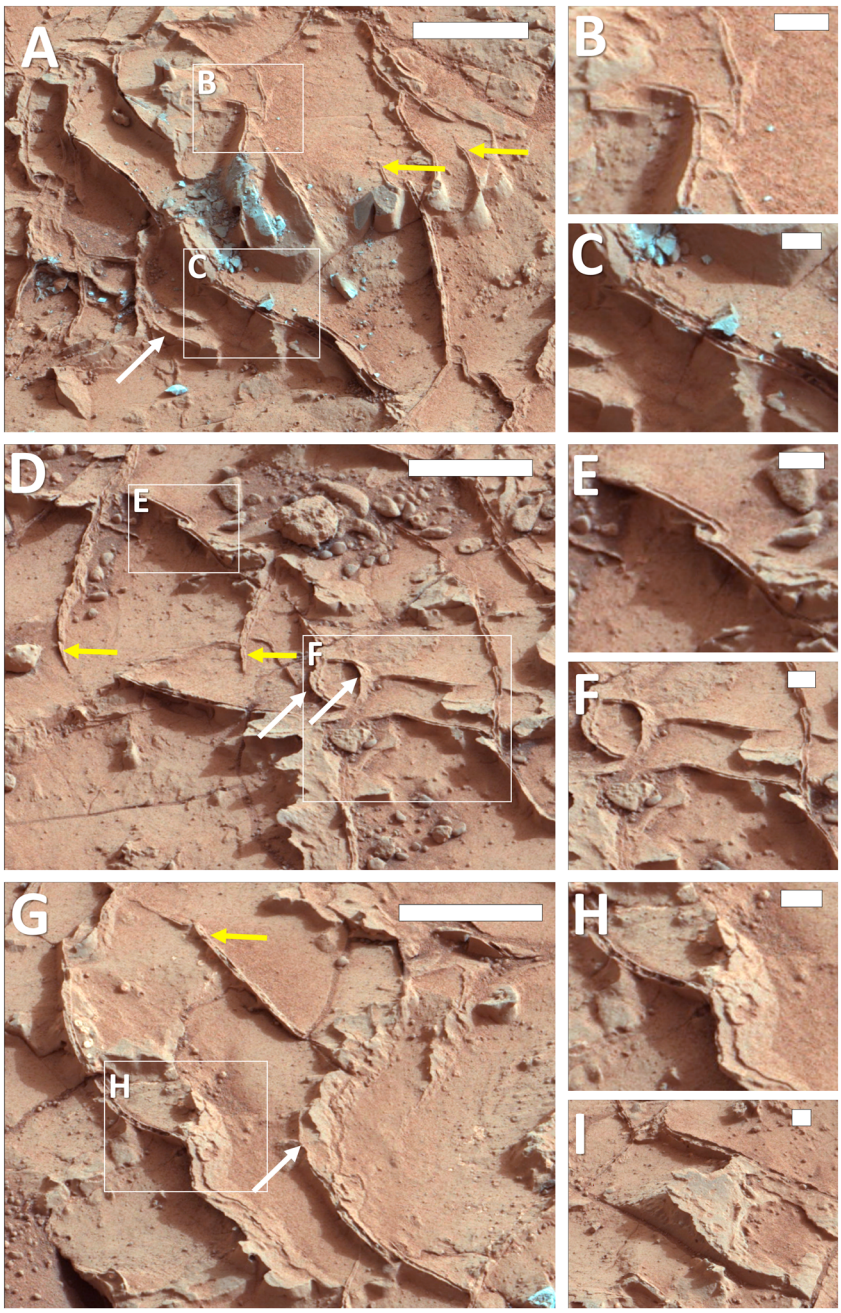

Figure 5. Insets showing details of raised ridge morphology with frames from white-balanced rover-perspective mosaic mcam00885, sol 164. Scale bars for Figures 5a, 5d, and 5g are 5 cm, scale bars for insets are 1 cm. Exposed grey rock surfaces were broken by the rover wheel. Yellow arrows highlight spindle-shaped cracks with tapered termini, white arrows highlight curvilinear features for comparison to Figure 6. (a–c) The isopachous cement lining that creates parallel-sided ridges outlining the cracks, and sometimes, as in Figure 5c, the multiple cement layers within the cracks. (d) The cracks are short and taper rapidly into a spindle shape. (e) Two cracks that appear to bend toward each other, indicating that the cracks all formed in one stage and traced planes of weakness in the rock. (f) The nonpolygonal nature of the cracks and resulting variety of crack intersection angles. (g) Multiple cracks that transition from near-vertical to subhorizontal spatial orientations. (h) An intersection between a near-vertical crack and a subhorizontal crack. (i) A ramped feature that appears to be a subhorizontal raised ridge preserved because of the resistant cement.

up to 50 cm, and widths range between 1.1 mm and 5.6 mm, averaging 2.6 mm. Terminations of the ridges, where visible, are tapered to a spindle-shaped point. Raised ridges do not form discrete polygons; where they do intersect, it is at an arbitrary variety of angles (Figures 5d–5f). The two-dimensional morphology of ridge exposures range from straight to sinuous (e.g., Figure 5). In some cases, adjacent ridges turn toward each other near the termini (e.g., Figure 5e).

Projection of raised ridges above the mudstone surface resulting from resistant crack-filling cement enables viewing of original crack orientation in three dimensions. Ridges range from vertical to subhorizontal in dip and are curviplanar; several ridges are observed transitioning from subvertical dip angles to subhorizontal dip angles that reflect crack intersections at oblique angles (Figures 5f–5h). Additionally, a variety of erosionally resistant, gently sloped features, marked by parallel bands morphologically similar to ridge cement, are visible in the mudstone up to a couple of centimeters above the surface and are interpreted as exhumed subhorizontal crack fills (e.g., Figures 5h and 5i).

As noted, these raised ridges reflect initial cracks that are currently filled with two to four layers of erosionally resistant infill. The crystal size of this cement infill is not visible, even at Mars Hand Lens Imager scales of 15–20 μm/pixel. The outermost cement, which represents the boundary between the sediment and the initial crack wall, is approximately 1 mm thick (measured normal to the crack surface) and has consistent thickness on all walls within individual raised ridges regardless of local curvature (i.e., it is an isopachous cement coating [*Pettijohn and Potter*, 1964]). The thickness of the cement varies in different ridge sets, from 0.6 mm to 1.2 mm (averaging 1.0 mm), but does not vary within individual ridges; within a given crack, the precipitation was isopachous. When two ridges intersect, this resistant cement continuously lines the edges of the intersecting features, regardless of the orientation of the initial cracks (e.g., Figure 5b). No evidence is seen for detrital sediment infilling of the cracks.

The APXS, ChemCam, and CheMin instruments onboard *Curiosity* were used to explore the composition of the resistant cement fill relative to the Sheepbed mudstone [*Grotzinger et al*., 2014; *McLennan et al*., 2014; *Vaniman et al*., 2014; Léveillé et al., submitted manuscript, 2014]. The ChemCam instrument (laser-induced-breakdown spectroscopy) has a spot size of about 0.5 mm and therefore was able to target laser shots along the outermost cement layer of the McGrath raised ridge target. Those analyses indicated that the outermost cement layer of the McGrath raised ridge is enriched in Mg, somewhat enriched in Li, and depleted in Al relative to the rest of the mudstone (Léveillé et al., submitted manuscript, 2014). The APXS has a 2.25 cm^2 spot area and also analyzed the subhorizontal McGrath target, finding that the ridge was enriched in Mg and Fe and that these were both correlated to enriched Cl relative to the Sheepbed mudstone [*McLennan et al*., 2014]. Additionally, the CheMin X-ray diffraction instrument analyzed two samples within the Sheepbed unit, neither of which contained a visible component representing the raised ridges. The Cumberland target, however, contained a notable contribution from nodules and hollow nodules, which appears to be reflected in a several percent increase in akaganeite (an iron oxide-hydroxide/chloride mineral) and magnetite relative to the John Klein drill hole, only about 2 m away [*McLennan et al*., 2014; *Vaniman et al*., 2014; *Stack et al*., 2014]. Based on these observations, it has been suggested that the resistant cement may be composed of akaganeite, magnetite, and/or some authigenic smectitic clay component, such as griffithite [*Grotzinger et al*., 2014; *McLennan et al*., 2014; *Vaniman et al*., 2014; Léveillé et al., submitted manuscript, 2014].

5. Discussion

Any proposed formation model must account for these observations: (1) Crack networks—as defined by their erosion-resistant infill—penetrate the mudstone, are spatially restricted, and transition laterally into high concentrations of nodules and hollow nodules or featureless mudstone; (2) individual cracks are curviplanar in three dimensions and crosscut stratigraphic contours; and (3) after opening, the cracks are filled with multiple generations of isopachous cement.

5.1. Origin of Raised Ridges

5.1.1. Formation Environment

Raised ridges within the Sheepbed mudstone appear to have originated as early diagenetic cracks within the mudstone. Their present morphology, as elevated ridges, is based on preferential erosion of the surrounding sediment relative to the crack fill (e.g., Figure 5b). The observation that cement continuously traces crack edges even when two cracks intersect demonstrates that the cracks were open before the cement layer

began to precipitate within open void space (Figure 5b). Apparent spatial clustering of both nodular features [*Stack et al*., 2014] and raised ridge networks suggests that either the distribution of one feature controlled the distribution of the other (for instance, via a change in mudstone rheology caused by the formation of one of the features) or that these are penecontemporaneous structures [e.g., *Calver and Baillie*, 1990; *Duck*, 1995]. In either case, crosscutting relationships indicate that both nodular features and raised ridges had formed and mineralized prior to formation of late-stage, sulfate-mineralized fractures (the sulfate-mineralized fractures clearly cut through raised ridges and through nodules, shown in Figure 2) [*Grotzinger et al*., 2014; Nachon et al. submitted manuscript, 2014]. If raised ridges and nodules are penecontemporaneous structures, we must examine the possibility that nodules and raised ridges share a common diagenetic environment.

In addition to their distribution, a critical observation that may constrain the origin of the raised ridge features is that the cracks that comprise raised ridge networks are short and curviplanar and have narrow to spindle-shaped terminations in three dimensions. This style of short, spindle-ended cracking occurs prior to complete lithification of the sediment [*Burst*, 1965; *Calver and Baillie*, 1990]. Additionally, cracks cross stratigraphic contours and intersection at arbitrary angles that do not form polygons (Figure 5). Polygonal cracking typically develops in response to internal, contractional stresses within the sediment (e.g., dewatering [*Shorlin et al*., 2000] or cooling [*Peck and Minakami*, 1968]) wherein the polygonal morphology acts to minimize stresses within the material. Because nonorthogonal, irregular crack intersections do not minimize stress, irregular crack orientations are typically interpreted to have formed quickly, exploiting inhomogeneities within the sediment [*Lachenbruch*, 1962; *Sletten et al*., 2003]. Furthermore, the extension of irregular intersections in three dimensions, the curviplanar morphology of cracks which result in transitions from subvertical to subhorizontal orientations, and the presence of cracks that crosscut stratigraphic contours (i.e., cracks do not appear to either terminate or originate at common bedding planes) all indicate crack formation in the subsurface [*O'Connor*, 1972; *Horodyski*, 1976; *Plummer and Gostin*, 1981], where overburden pressures are sufficient to equalize vertical and horizontal stresses.

5.1.2. Comparison With Terrestrial Early Diagenetic Cracks

Combined, these lines of evidence suggest that raised ridges originated as subplanar cracks, or voids, contained fully within the sediment. This model is very different from the most familiar mode of early diagenetic fracturing on Earth—the formation of desiccation cracks. Desiccation cracks form at the sediment-air interface because water loss leads to contraction of the sediment [*Lachenbruch*, 1962; *Plummer and Gostin*, 1981]. Such desiccation features originate at a discrete sedimentary surface (a future bedding plane) and extend vertically into the subsurface, forming a wedge shape that narrows and ultimately terminates at some depth (often at variable depths) within the sediment [*Weinberger*, 1999]. Although early stages of crack formation may be recognized by the presence of short, isolated cracks (e.g., "incomplete mudcracks" [*Plummer and Gostin*, 1981]), these initial cracks typically expand and intersect in a polygonal pattern to minimize contractional stresses within the surface layers [*Sletten et al*., 2003]. Regardless of the extent to which this ultimate, polygonal morphology is reached, desiccation cracks that enter the rock record are invariably filled by detrital sediment from the sediments that directly overlie the desiccated strata [*Pettijohn and Potter*, 1964]. Indeed, desiccation cracks in the rock record are recognized by the sediments that fill them. This is in sharp contrast to the Sheepbed cracks, which were filled with neither fine-grained Sheepbed sediment nor relatively coarse-grained sands from the Gillespie Lake sediment but instead show multiple isopachous cement layers. Furthermore, the Sheepbed cracks are curviplanar in three dimensions and do not form polygons or terminate along bedding planes.

Although less common, subaqueous cracking of sediments is not unknown in terrestrial environments (e.g., Figure 6). Subaqueous crack formation was first recognized by White [1961], who suggested that subaqueous cracks could result from in situ salinity changes in clay colloids leading to fabric collapse and then contraction and tighter packing of the clays. This process generates crack-shaped voids that are filled with the displaced fluids (Figure 7a). The term "syneresis" was applied to these cracks to refer to the contractional stresses within the sediment that resulted during fabric collapse within the clay [*White*, 1961]. The potential for saline fluids to result in such volumetric shrinkage was experimentally confirmed by *Burst* [1965], and the resulting features share many commonalities with raised ridges in the Sheepbed mudstone. For instance, syneresis cracks tend to be short and straight to sinuous, are generally spindle-shaped with tapering termini [*O'Connor*, 1972; *Plummer and Gostin*, 1981], form in the very shallow subsurface (all predate sediment compaction), and crosscut

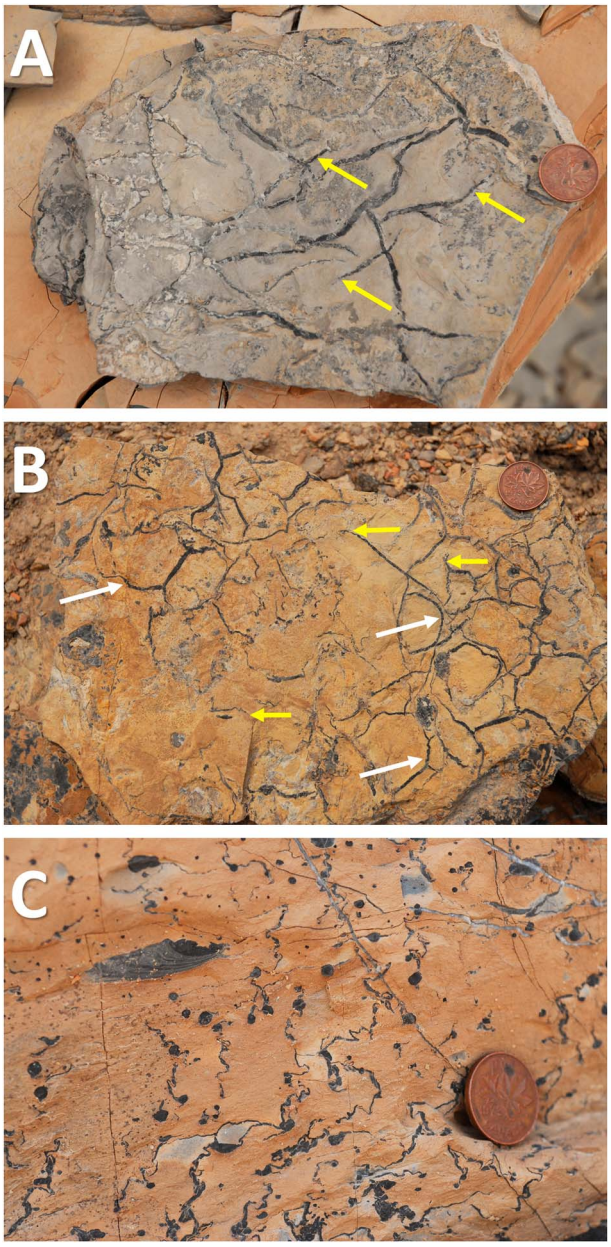

Figure 6. Proterozoic molar tooth structures from the Helena formation in the Belt Supergroup, MT, USA. Coin is 19 mm across for scale. (a and b) Preserved bedding planes with short, curvilinear, spindle-shaped cracks. Yellow arrows highlight spindle-shaped cracks with tapered termini, white arrows highlight curvilinear features for comparison to Figure 5. These crack morphologies are very comparable to the raised ridge crack morphologies, although the cement is not resistant to erosion in this case. Note curvilinear cracks and irregular clustered distribution in Figure 6b. (c) A cross section of molar tooth ribbons and blobs. Note interfingering transition between ribbon and blob facies and horizontal-to-vertical transitions of ribbons.

bedding planes [*Horodyski*, 1976; *Plummer and Gostin*, 1981]. Additionally, the presence of a significant amount of smectite clays within the Sheepbed mudstone [*McLennan et al*., 2014; *Vaniman et al*., 2014] suggests that environmental conditions may have been favorable for saline-fluid-based syneresis (Figure 7a).

More recently, several additional formation processes for syneresis cracks have been proposed. In one alternative, syneresis-like features result from tensional stresses imposed upon sediment from an external source [*Cowan and James*, 1992; *Pratt*, 1998a, 1998b; *Bishop et al*., 2006]. Cracks in one subcategory that clearly form by this mechanism, termed "diastasis" cracks [*Cowan and James*, 1992], are subplanar, subvertical, often well-aligned spindle-shaped cracks that form in clay-rich, cohesive layers as these layers are placed under tension from wave-driven motion of overlying and underlying sandy, or less cohesive, layers. Rupture of the cohesive layer permits rapid infilling of diastasis cracks via injection of less cohesive sediment from either above or below the cohesive layer. A critical observation leading to the interpretation of diastasis cracks, however, is the presence of systematic crack orientations resulting from a directed tensional stress field. Raised ridges within the Sheepbed mudstone show no such preferred orientation (see Figure 3), suggesting that diastasis is an unlikely mechanism of formation. A similar formation mechanism that does not require layered sediments suggests that these cracks could open due to shaking of the sediment from nearby seismic activity (possibly due to landslides or impacts in this case) even in homogeneous cohesive material [*Pratt*, 1998a, 1998b]. This mechanism would not produce aligned cracks and so cannot be ruled out for the raised ridge features.

In a third scenario, syneresis-like cracks are inferred to result from the production of gasses within sedimentary pore fluids, creating localized dilational stresses within the sediment. On Earth, Proterozoic "molar-tooth" structures are typically interpreted to have formed this way [*Smith*, 1968; *Plummer and Gostin*, 1981; *Furniss et al*., 1998]. Predictable behavior between the production (or exsolution) of gas within pore fluids and the surrounding sediment [*Terzaghi*, 1944; *Mitchener and Torfs*, 1996; *Pollock et al*., 2006; *Stack et al*., 2014] creates structures that provide an interesting

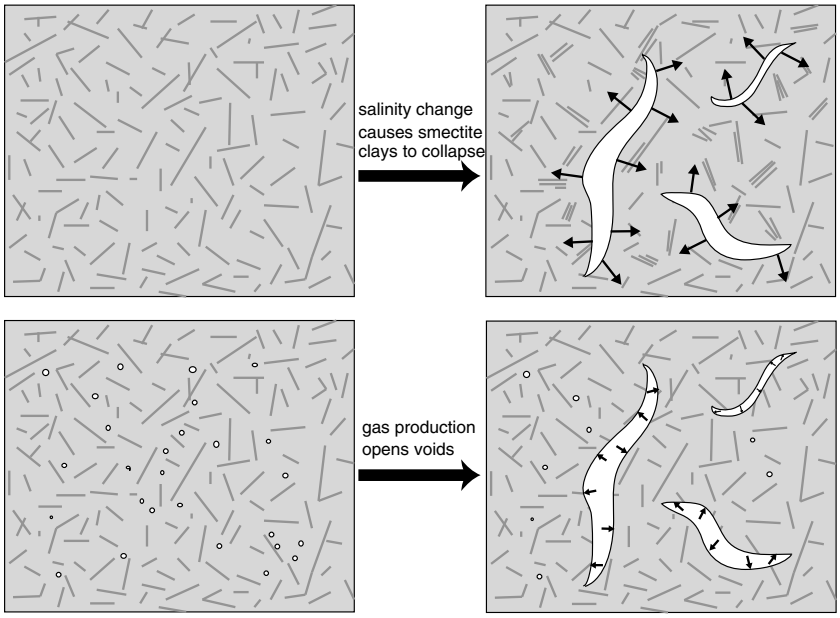

Figure 7. Schematic showing possible formation mechanisms for syneresis crack formation. (a) A change in pore fluid chemistry that causes collapse of smectite clay interlayers, causing volumetric compaction of the sediment, which opens syneresis cracks. (b) A gas production process such that if the gas becomes trapped, it can create void spaces within the mudstone, which could form both hollow nodules and syneresis or raised ridge shapes.

comparison to the morphology of primary void spaces within the Sheepbed mudstone. The primary parameter in determining the behavior of gasses within unconsolidated substrate is the cohesive strength of the sediment [*Terzaghi*, 1944], which commonly reflects a combination of grain size and composition. Composition is critical because the presence of >15% clay minerals within the sediment has been shown to substantially increase its cohesive strength [*Mitchener and Torfs*, 1996]. Once gasses form bubbles that are larger than interparticle void space, these bubbles will provide dilational stresses that deform and compact the surrounding sediment. Because gasses will tend to rise and escape, grain-scale inhomogeneities will be exploited and favor the upward movement of gas. In the case of poorly consolidated sediments, upward migration of gas bubbles will often result in dewatering and an increase in the consolidation of sediments. In the case of higher strength sediments (such as cohesive and clay-rich sediments), gas bubbles will tend to be trapped as consolidation of grains along the bubble margin increases local sediment strength. Under these conditions, crack formation can occur when gas pressures exceed the local sediment yield strength, and cracks will commonly propagate in a range of orientations, from vertical (denoting the favored orientation for gas escape) to horizontal (denoting a common direction of weakness within layered sediment) [*Pollock et al*., 2006].

Exsolution of gasses within substrate pore space has recently been proposed as a mechanism for the formation of nodules and hollow nodules within the Sheepbed mudstone [*Stack et al*., 2014]. A mechanism of void formation resulting from release of sediment gasses can plausibly explain both the formation of early diagenetic hollow nodules [*Stack et al*., 2014] and cracks associated with the raised ridges. Differences in the morphology of gas-induced structures may reflect either differences in the rate of production of gasses within the sediment or spatial differences in the cohesive strength of the sediment [*Pollock et al*., 2006]. *Stack et al*. [2014] further suggest a combination of these last two mechanisms of crack formation, in which release of pore fluid gasses may plausibly be related to the propagation of impact-induced seismic waves during deposition of the Yellowknife Bay formation. In this scenario, complex interference patterns could produce zones of greater or lesser seismic pressure, which might affect the extent to which pressure-induced degassing occurs and thereby control the spatial distribution of nodular features and crack networks. Similarly, slight changes in the cohesive strength of the substrate, resulting from either differential compaction or spatial differences in clay content, may be reflected in the spatial distribution of gas-induced features.

Formation of raised ridges as curviplanar voids in the subsurface formed via gas expansion supports the observations of crack clustering and the crosscutting of stratigraphic contour intervals. Similarly, such a mechanism supports the varied orientation of observed features, which presumably reflect lithologic zones of weakness and inhomogeneities in the sediment (Figure 3). Finally, the observation of multiple clusters of raised ridges directly beneath and, in one case, intersecting the Gillespie Lake member suggests that crack formation must have occurred penecontemporaneously with or soon after deposition of the basal Gillespie Lake sandstone. These observations suggest that crack formation occurred prior to burial-induced dewatering and provide the possibility that the relatively coarse-grained Gillespie Lake member may have provided critical overburden pressure necessary to increase gas pressures during exsolution of gasses within Sheepbed pore fluids.

5.2. Lithification of Raised Ridges

Regardless of the formation mechanism of subplanar cracks and voids within the Sheepbed mudstone, it is necessary to discuss their mechanism of preservation. Fine-grained sediment can preserve cracks formed during or shortly after sediment deposition under several distinct conditions. First, there is a possibility that sediment is sufficiently lithified via early cementation so that it can retain otherwise unsupported void space. However, more commonly, the void space fills with sediment or detritus or is propped open by cement that occludes porosity [*Halley and Schmoker*, 1983]. In general, if cracking occurs at the sediment-water (or sediment-air) interface, cracks will typically be filled with sediment from above [*Pettijohn and Potter*, 1964]. Similarly, subaqueous shrinkage cracks formed via diastasis will typically be filled with sediment injected from less cohesive sedimentary units either directly above or below the cracked horizon [*Cowan and James*, 1992]. By contrast, subaqueous cracks on Earth that originate from gas expansion are commonly filled with in situ mineral precipitates [*Furniss et al*., 1998; *Bishop et al*., 2006; *Pollock et al*., 2006]. In the case of the Sheepbed features, after crack formation, voids were filled by a succession of isopachous cement layers. The initial erosion-resistant cement layer is approximately 1 mm thick, measured normal to the crack surface regardless of local curvature, and thus provides an equal-thickness coating on all available surfaces. Isopachous coatings indicate that the cement was precipitated in a phreatic, or water-saturated, environment [e.g., *Longman*, 1980; *Amieux et al*., 1989]. Erosionally resistant isopachous cement is the defining attribute of the raised ridges throughout the observed Sheepbed member and likely reflects pore fluid chemistry, or the chemical interaction between pore fluids and released gasses, at the time of crack formation.

After this initial cement was deposited, an erosionally less-resistant cement precipitated within the remaining void space, further infilling and occluding the porosity. In wider cracks, this was followed by another erosionally resistant cement layer, and if residual porosity remained, it was occluded by a final, erosionally less-resistant cement. This type of layered and laterally repeated cementation of voids is common on Earth where it is utilized in "cement stratigraphy" [*Evamy*, 1969; *Meyers*, 1991], a methodology where sequences of different cement layers are traced on a regional scale and used to map ancient groundwater or pore water systems [*Grover and Read*, 1983; *Kaufman et al*., 1988]. Different cement layers are usually attributed to evolving fluid chemistries and sometimes related to distinct fluid flow events [*Meyers*, 1974; *Meyers and Lohmann*, 1985; *Dorobek*, 1987]. In the raised ridges, variation in erosional resistance of successive cement layers most likely indicates a change in cement composition that reflects changes in the pore fluid chemistry. Such interpretation is supported by the ChemCam observation that the outermost resistant cement is enriched in Mg and depleted in Al relative to the interior layers (Léveillé et al., submitted manuscript, 2014). At present, it is impossible to constrain the exact timing of these different cement layers. Once the initial erosionally resistant cement was precipitated, it would have acted to reinforce void walls, permitting voids to potentially remain open for extended periods of time. The absence, however, of significant calcium sulfate mineralization within the cracks suggests that cementation of the raised ridges was complete prior to late-stage hydrofracture of the Yellowknife Bay formation [*Grotzinger et al*., 2014; Nachon et al. submitted manuscript, 2014].

5.3. Formation Summary and Comparison With Earth Analogs

Key first-order interpretations that we can derive from observations of the raised ridges are the following: (1) the cracks formed during early diagenesis of the Sheepbed mudstone; (2) the cracks formed in a near-isotropic stress environment created by overburden pressure from overlying sediments; (3) mineral precipitation within the crack initiated soon after crack formation in a water-saturated environment and proceeded with a series of precipitated cements of differing mineralogy and/or resistance to erosion; and (4) the morphology

and distribution of the Sheepbed cracks matches the characteristics identified for syneresis cracks, which form via sediment contraction with pore fluid salinity changes, mechanical shaking, exsolution of pore fluid gasses, or some combination thereof.

Having established this set of constraints concerning the early diagenetic, subsurface, pore fluid-saturated environment in which the raised ridges formed and filled, the remaining challenge is to evaluate the set of syneresis crack formation hypotheses for applicability to the Sheepbed member structures based on Earth analogs. Although isolating specific crack formation mechanisms for subaqueous/shallow burial conditions is difficult for ancient sedimentary rocks, even on Earth, because of the absence of good modern analogs [e.g., *Smith*, 1968; *Frank and Lyons*, 1998; *Furniss et al*., 1998; *James et al*., 1998; *Pratt*, 1998a; *Marshall and Anglin*, 2004], the observations of the Sheepbed member and the restricted set of plausible environments on Mars help constrain the likely possibilities.

The most accepted hypotheses for syneresis crack formation, as discussed, include (1) pore fluid salinity changes causing clay layer collapse and volumetric shrinkage of the sediment, (2) mechanical shaking of the sediments causing tensional stresses, and (3) gas production in the sediment creating dilational stresses. Key observations in the Sheepbed unit that must be explained by the specific formation hypothesis include the clustered, irregular distribution of raised ridges, the lack of a preferred ridge orientation, and the cement (rather than sediment) crack infill.

Pore fluid salinity changes causing clay layer collapse create syneresis cracks preferentially in clay-rich areas [*White*, 1961; *Burst*, 1965]. This method of crack formation could create a clustered distribution of raised ridges if clay-rich zones were heterogeneously distributed in the mudstone. Although this is not specifically constrained by *Curiosity*'s observations, since only two holes were drilled and sampled for XRD mineral compositions, it is plausible given the presence of smectite within the unit and the compositional differences between the John Klein and Cumberland drill sites [*McLennan et al*., 2014; *Vaniman et al*., 2014]. Preferred ridge orientations would not be expected for this formation mechanism as cracks would follow inhomogeneities in the sediment. Although cracks formed in this manner on Earth are usually preserved by sediment infill rather than precipitated cements, this mechanism for forming void spaces cannot be ruled out for the Sheepbed raised ridges.

Earthquake-induced shaking [*Cowan and James*, 1992; *Fairchild et al*., 1997; *Pratt*, 1998a, 1998b] or repeated wave action [*James et al*., 1998; *Bishop et al*., 2006] mechanically breaking up cohesive but unlithified sediments have also been used to explain syneresis crack formation. There is no evidence for wave-induced sedimentary structures in the Sheepbed mudstone [*Grotzinger et al*., 2014], and seismicity is rare on Mars [*Anderson et al*., 1977; *Golombek et al*., 1992]; however, impact-induced shaking could be a possible Martian alternative for mechanical shaking of sediments to form syneresis cracks. The clustered distribution of cracks in the Sheepbed could be based on slight lithological differences in the sediment. However, cracks formed by this mechanism are inevitably preserved in ancient rocks by sediment infill rather than mineral precipitation, so this is not a favored hypothesis for the Sheepbed raised ridges.

Whereas both salinity changes and mechanical shaking could viably have occurred during deposition of the Sheepbed mudstone, the most distinctive characteristic of the raised ridges relative to the majority of terrestrial syneresis cracks is that they are filled with cement rather than sediment [e.g., *White*, 1961; *Pettijohn and Potter*, 1964; *Burst*, 1965; *Cowan and James*, 1992]. The one notable terrestrial example of a class of syneresis cracks where cement rather than sediment fills the voids is called molar tooth and the production of these structures is most often attributed to gas production in the subsurface [*Bauerman*, 1885; *Furniss et al*., 1998; *Pollock et al*., 2006]. This gas formation hypothesis predicts an irregular distribution of syneresis cracks and other diagenetic morphologies based on minor differences in sediment lithology and does not predict a preferred ridge orientation. Furthermore, molar tooth cracks are always filled with cement; the cements that fill molar tooth cracks precipitate so early that sometimes they are reworked during current scouring, leaving void-fill present as sedimentary clasts in immediately overlying beds [*Smith*, 1968; *O'Connor*, 1972; *James et al*., 1998; *Bishop et al*., 2006]. In terrestrial environments, these void-filling cements are primarily calcite, although in at least one location, early diagenetic saponite (presently talc) likely precipitates as cement [*Tosca et al*., 2011]. Raised ridges within the Sheepbed member similarly contain early diagenetic cement infill, potentially smectite, and/or a chlorite phase such as akaganeite [*McLennan et al*., 2014; Léveillé et al., submitted manuscript, 2014].

The multiple morphologies of terrestrial molar tooth textures, all interpreted as due to gas production in the subsurface, invite further comparison with the diagenetic textures in the Sheepbed unit. The most common molar tooth morphologies are "ribbons" and "blobs" [*O'Connor*, 1972]. In scale and morphology, ribbons, the syneresis-like components of molar tooth structure, are very similar to the raised ridges in the Sheepbed unit; they are narrow, at times sinuous, spindle-terminated cement-filled fractures and they are observed to transition between horizontal and vertical dimensions (Figure 6) [*O'Connor*, 1972; *Horodyski*, 1976; *Plummer and Gostin*, 1981]. Molar tooth blobs are typically millimeter- to centimeter-scale spheroidal pockets, suggested to have formed as gas bubbles, either interfingered with the ribbons or in separate clusters, and filled with the same calcite cement [*O'Connor*, 1972; *Pollock et al*., 2006]. These blobs may be comparable to the early diagenetic hollow nodules described in the Sheepbed unit as rimmed, erosion-resistant, spheroidal structures about 1.2 mm in diameter that are clustered in some locations and laterally transition into raised ridge clusters [*Grotzinger et al*., 2014; *Stack et al*., 2014]. Both the ribbon and blob morphologies are explained by gas production in mudstone, where slight variations in lithology and cementation or in localized gas production have been used to explain transitions between unaltered mudstone, blobs, and ribbons [*Pollock et al*., 2006]. These features are illustrated in Figure 6 with arrows pointing out the features that are also visible in the Sheepbed raised ridges (Figure 5). It is important to note that the cements that fill molar tooth structures are not isopachous and are not resistant relative to the surrounding rock, so the three-dimensional structure (including the subvertical to subhorizontal transitions) is only visible when looking at the rock in cross section (e.g., Figure 6c). However, comparison of the two-dimensional crack shapes reveals the similarity in spindle terminations, curvilinear crack geometry, clustered distribution, and transitions between morphologies. In summary, although the composition and style of the infilling cement in the Sheepbed unit is distinct from that usually found in molar tooth structures, the analog is unique because it is filled by cement rather than sediment and because it suggests that gas formation or a similar single formation mechanism could potentially create more than one of the early diagenetic morphologies in the Sheepbed unit. This would fit with the observations of lateral transitions between diagenetic textures.

6. Summary

The following results have been drawn from this study:

1. Resistant cement-filled cracks (raised ridges) in the Sheepbed mudstone were observed and mapped using imagery from the *Curiosity* rover.
2. The raised ridges are shown to be early diagenetic features based on lateral transitions with other diagenetic textures. Later sulfate-filled veins crosscut these early diagenetic features.
3. Comparison with analogous early diagenetic mud crack morphologies indicates that the raised ridges are syneresis cracks (subaqueous shrinkage cracks).
4. Isopachous cement fills with differing erosion resistance likely represent a series of different cements indicating changing pore fluid chemistries within the phreatic zone.
5. Syneresis crack formation mechanisms viable in the Sheepbed unit include pore fluid salinity changes causing volumetric shrinkage of smectitic clay fabrics, impact-induced mechanical shaking, and gas production.
6. Proterozoic molar tooth structures, formed by gas production, provide an intriguing analog for the raised ridges because they (1) are cement-filled and (2) have multiple morphologies comparable to the diagenetic morphologies in the Sheepbed mudstone.

Appendix A

A1. Description of Processing of Mastcam Images

Mastcam images are acquired at 12 bits, with the noise level captured by the least significant bit. The data are then converted to 8 bit using an 11 bit lookup table. Although several tables exist, a modified square root table (Figure A1) was used to encode the vast majority of the images. This table will encode multiple input values to a single output value, approximating the statistical variation of the signal. After encoding, the images are stowed within the camera's large buffer memory. When downlinked, the images can be compressed with a predictive lossless compressor or more normally with a JPEG compressor with selectable quality factor. Typically, quality factors of 85 or higher are used for geology targets.

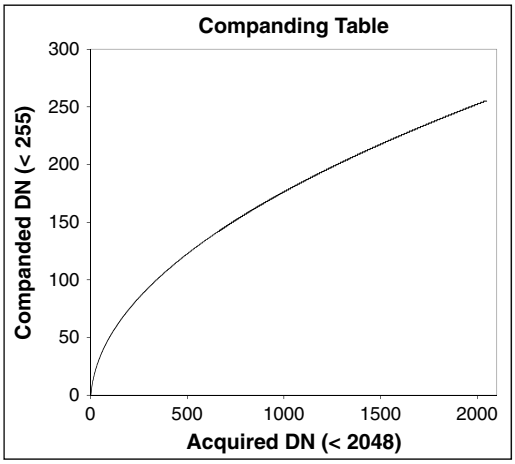

Figure A1. Modified square root companding table used to encode the images in *Curiosity*'s Mastcam buffer. Encodes multiple input values into a single output value to approximate the signal's statistical variability.

A1.1. Radiometric Ground Image Processing

Radiometric ground image processing proceeds as follows: images are first decompressed and then expanded back to their original dynamic range using an inverse of the encoding table; no interpolation is applied in an attempt to recover the full variance around each mean value. For computational convenience, these data are stowed in 16 bit words. A temperature-dependent correction is then applied to adjust for thermally generated electrons (noise). For short exposures, an electronic shutter smear correction is applied (generally, the images used in this study did not need this correction). A flat field correction is then applied to cancel lens brightness nonuniformity. The final photometric process is to adjust for detector sensitivity to create radiance images. Images that have gone through this processing are available through the Planetary Data System (PDS) as Reduced Data Records, designated by the letters in the Picture ID *_DRXX.IMG.

A1.2. Geometric Image Processing

Geometric processing proceeds as follows: each image is geometrically linearized to remove camera lens distortion and prepare the image for further geometric processing. Images at this stage of processing are also available from the PDS as *_DRLX.IMG products. This processing is further described in the Mastcam/MAHLI/MARDI Software Interface Specification [*NASA-JPL*, 2013].

Images acquired as stereoscopic sets (pairs or larger mosaics) are aggregated into a separate directory and processed by a modification of the Ames Stereo Pipeline created by Mastcam Co-Investigator Laurence Edwards. This processing includes five steps. First, relevant acquisition parameters are extracted from each image's metadata, its analogous pair is identified, and the images are converted from the PDS format to an internal format. Second, an image alignment is performed along with a reprojection transformation using the camera models (required because the two Mast cameras have disparate focal lengths). By default, the alignment and reprojection produces an epipolar aligned image pair, although other schemes can be chosen for unusual imaging geometries. Third, stereoprocessing of each image pair is completed: a filter is applied to each image that enhances edges and reduces sensitivity to differing lighting conditions. A pyramidal correlation scheme utilizing three or more reduced scale versions of each image and a fixed-sized correlation window quickly generate disparity search constraints. The initial search constraints are used as input to an integer correlator stage operating on the full resolution images. The results from the integer

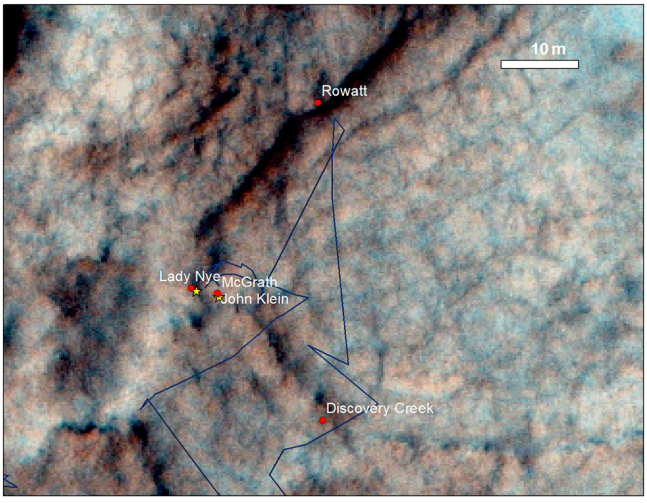

Figure A2. Map showing locations of all raised ridge targets (red circles) that were shot by the ChemCam laser-induced breakdown spectroscopy (LIBS) instrument. Yellow stars show drill sites, Cumberland on the left and John Klein on the right. Dark blue path represents rover traverse.

correlator are in turn utilized by a subpixel correlator stage generating dense high-resolution disparity maps with subpixel accuracy, and then automated pruning of bad correlations, based on a bidirectional consistency check and numerical confidence levels computed by the correlation software, occurs at each stage. Fourth, the final subpixel disparity map is interpolated and smoothed, and the camera models are used to generate 3-D coordinates for each pixel where a valid match was determined. Fifth, the output from each run includes intermediate processing images used in correlation, a pointcloud, XYZ maps, and mesh models in SGI OpenInventor format, with textures derived from the higher resolution camera image data (right eye). For multiple image stereo mosaics, an index mesh collection file is also created. All 3-D data are in rover navigation coordinates.

The output of the stereo processing can be viewed in Triangulated Integrated Network (TIN) format in software capable of reading SGI *.iv files. For further processing into Digital Elevation Models (DEMs) and associated orthographic map projected images, the TIN to DEM conversion capability of the Ames Research Center Antares visualization software is employed. This software resamples the mesh into height and texture raster images, allowing the user to specify the sampling interval, interpolating where necessary. The final output consists of two GeoTiff image files: a signed 32 bit DEM and a 24 bit (8 bits per channel) color texture image, both in orthographic projection, with labels in Geotiff format and local site coordinates.

A2. Location of Raised Ridges Targeted by ChemCam

Raised ridge clusters outside of the range of Figure 3 that were targeted by ChemCam include Rowatt and Discovery Creek. The locations of these images in the Sheepbed unit are shown in Figure A2 along with the rover traverse through Yellowknife Bay.

Acknowledgments

This work was supported by NASA Mars Science Laboratory grant 1449659 to J.P.G. We are grateful to our Mars Science Laboratory science team colleagues for helpful discussions and particularly thank science team members J. Schieber and D. Oehler for helpful comments on an earlier version of this manuscript. Comments from two anonymous reviewers further improved this manuscript.

References

Amieux, P., P. Bernier, and R. Dalongeville (1989), Cathodoluminescence of carbonate-cemented Holocene beachrock from the Togo coastline (West Africa): An approach to early diagenesis, *Sediment. Geol.*, *65*(3), 261–272.

Anderson, D. L., W. Miller, G. Latham, Y. Nakamura, M. Toksöz, A. Dainty, F. Duennebier, A. Lazarewicz, R. Kovach, and T. Knight (1977), Seismology on Mars, *J. Geophys. Res.*, *82*(28), 4524–4546, doi:10.1029/JS082i028p04524.

Arvidson, R. E., et al. (2014), Ancient aqueous environments at Endeavour crater, Mars, *Science*, *343*(6169), doi:10.1126/science.1248097.

Bauerman, H. (1885), Report on the geology of the country near the forty-ninth parallel of North latitude West of the Rocky Mountains, Report of Progress 1882–1884, Part B, Geological Survey of Canada (1885), pp. 1–42.

Bell, J., A. Godber, M. Rice, A. Fraeman, B. Ehlmann, W. Goetz, C. Hardgrove, D. Harker, J. Johnson, and K. Kinch (2013), Initial multispectral imaging results from the Mars Science Laboratory Mastcam investigation at the Gale crater field site, paper presented at 44th Lunar and Planetary Science Conference, Houston, Tex., 1417.

Bishop, J. W., D. Y. Sumner, and N. J. Huerta (2006), Molar tooth structures of the Neoarchean Monteville Formation, Transvaal Supergroup, South Africa. II: A wave-induced fluid flow model, *Sedimentology*, *53*(5), 1069–1082, doi:10.1111/j.1365-3091.2006.00802.x.

Burst, J. F. (1965), Subaqueously formed shrinkage cracks in clay, *J. Sediment. Petrol.*, *35*(2), 348–353.

Calver, C. R., and P. W. Baillie (1990), Early diagenetic concretions associated with intrastratal shrinkage cracks in an upper Proterozoic dolomite, Tasmania, Australia, *J. Sediment. Res.*, *60*(2), 293–305.

Clark, B. C., et al. (2005), Chemistry and mineralogy of outcrops at Meridiani Planum, *Earth Planet. Sci. Lett.*, *240*(1), 73–94, doi:10.1016/j.epsl.2005.09.040.

Cowan, C. A., and N. P. James (1992), Diastasis cracks: Mechanically generated synaeresis-like cracks in Upper Cambrian shallow water oolite and ribbon carbonates, *Sedimentology*, *39*, 1101–1118.

Dorobek, S. L. (1987), Petrography, geochemistry, and origin of burial diagenetic facies, Siluro-Devonian Helderberg Group (carbonate rocks), central Appalachians, *AAPG Bull.*, *71*(5), 492–514.

Duck, R. W. (1995), Subaqueous shrinkage cracks and early sediment fabrics preserved in Pleistocene calcareous concretions, *J. Geol. Soc. London*, *152*, 151–156, doi:10.1144/gsjgs.152.1.0151.

Ehlmann, B. L., J. F. Mustard, C. I. Fassett, S. C. Schon, J. W. Head Iii, D. J. Des Marais, J. A. Grant, and S. L. Murchie (2008), Clay minerals in delta deposits and organic preservation potential on Mars, *Nat. Geosci.*, *1*(6), 355–358, doi:10.1038/ngeo207.

Ehlmann, B. L., J. F. Mustard, S. L. Murchie, J. P. Bibring, A. Meunier, A. A. Fraeman, and Y. Langevin (2011), Subsurface water and clay mineral formation during the early history of Mars, *Nature*, *479*(7371), 53–60, doi:10.1038/nature10582.

Evamy, B. (1969), The precipitational environment and correlation of some calcite cements deduced from artificial staining, *J. Sediment. Res.*, *39*(2), 787–793.

Fairchild, I. J., G. Einsele, and T. R. Song (1997), Possible seismic origin of molar tooth structures in Neoproterozoic carbonate ramp deposits, north China, *Sedimentology*, *44*(4), 611–636, doi:10.1046/j.1365-3091.1997.d01-40.x.

Frank, T. D., and T. W. Lyons (1998), "Molar-tooth" structures: A geochemical perspective on a Proterozoic enigma, *Geology*, *26*(8), 683–686, doi:10.1130/0091-7613(1998)026<0683:Mtsagp>2.3.Co;2.

Furniss, G., J. F. Rittel, and D. Winston (1998), Gas bubble and expansion crack origin of "molar-tooth" calcite structures in the Middle Proterozoic Belt Supergroup, western Montana, *J. Sediment. Res.*, *68*(1), 104–114.

Golombek, M. P., W. B. Banerdt, K. L. Tanaka, and D. M. Tralli (1992), A prediction of Mars seismicity from surface faulting, *Science*, *258*(5084), 979–981.

Grotzinger, J. P., and R. E. Milliken (2012), The sedimentary rock record of Mars: Distribution, origins, and global stratigraphy, in *Sedimentary Geology of Mars*, *SEPM Spec. Pap.*, vol. 102, edited by J. P. Grotzinger and R. E. Milliken, pp. 1–48, SEPM, Tulsa, Okla.

Grotzinger, J. P., et al. (2014), A habitable fluvio-lacustrine environment at Yellowknife Bay, Gale crater, Mars, *Science*, *343*(6169), doi:10.1126/science.1242777.

Grotzinger, J., et al. (2005), Stratigraphy and sedimentology of a dry to wet eolian depositional system, Burns formation, Meridiani Planum, Mars, *Earth Planet. Sci. Lett.*, *240*(1), 11–72, doi:10.1016/j.epsl.2005.09.039.
Grover, G., and J. Read (1983), Paleoaquifer and deep burial related cements defined by regional cathodoluminescent patterns, Middle Ordovician carbonates, Virginia, *AAPG Bull.*, *67*(8), 1275–1303.
Halley, R. B., and J. W. Schmoker (1983), High porosity Cenozoic carbonate rocks of south Florida: Progressive loss of porosity with depth, *AAPG Bull.*, *67*(2), 191–200.
Horodyski, R. J. (1976), Stromatolites of the upper Siyeh limestone (middle proterozoic), belt supergroup, Glacier National Park, Montana, *Precambrian Res.*, *3*(6), 517–536.
James, N. P., G. M. Narbonne, and A. G. Sherman (1998), Molar-tooth carbonates: Shallow subtidal facies of the Mid-to Late Proterozoic, *J. Sediment. Res.*, *68*(5), 716–722.
Kaufman, J., H. S. Cander, L. D. Daniels, and W. J. Meyers (1988), Calcite cement stratigraphy and cementation history of the Burlington-Keokuk Formation (Mississippian), Illinois and Missouri, *J. Sediment. Petrol.*, *58*(2), 312–326.
Knoll, A. H., and J. Grotzinger (2006), Water on Mars and the prospect of Martian life, *Elements*, *2*(3), 169–173.
Lachenbruch, A. H. (1962), Mechanics of thermal contraction cracks and ice-wedge polygons in permafrost, *Geol. Soc. Am. Bull. Spec. Paper*, *70*, 1–66.
Long, J. C. S., et al. (1996), *Rock Fractures and Fluid Flow: Contemporary Understanding and Applications*, 551 pp., National Academy Press, Washington, D. C.
Longman, M. W. (1980), Carbonate diagenetic textures from nearsurface diagenetic environments, *AAPG Bull.*, *64*(4), 461–487.
Maki, J., D. Thiessen, A. Pourangi, P. Kobzeff, T. Litwin, L. Scherr, S. Elliott, A. Dingizian, and M. Maimone (2012), The Mars Science Laboratory engineering cameras, *Space Sci. Rev.*, *170*(1–4), 77–93, doi:10.1007/s11214-012-9882-4.
Malin, M., M. Caplinger, K. Edgett, F. Ghaemi, M. Ravine, J. Schaffner, J. Baker, J. Bardis, D. DiBiase, and J. Maki (2010), The Mars Science Laboratory (MSL) mast-mounted cameras (Mastcams) flight instruments, paper presented at 41st Lunar and Planetary Science Conference, Houston, Tex., 1123.
Marshall, D., and C. D. Anglin (2004), CO2-clathrate destabilization: A new model of formation for molar tooth structures, *Precambrian Res.*, *129*(3–4), 325–341, doi:10.1016/j.precamres.2003.10.007.
McEwen, A. S., et al. (2007), Mars Reconnaissance Orbiter's High Resolution Imaging Science Experiment (HiRISE), *J. Geophys. Res.*, *112*, E05S02, doi:10.1029/2005JE002605.
McLennan, S., and J. Grotzinger (2008), The sedimentary rock cycle of Mars, in *The Martian Surface Composition, Mineralogy, and Physical Properties*, vol. 1, edited by J. Bell, 541 pp., Cambridge Univ. Press, New York.
McLennan, S. M. (2012), Geochemistry of sedimentary processes on Mars, in *Sedimentary Geology of Mars*, edited by J. Grotzinger and R. Milliken, 270 pp., SEPM, Tulsa, Okla.
McLennan, S. M., et al. (2005), Provenance and diagenesis of the evaporite-bearing Burns formation, Meridiani Planum, Mars, *Earth Planet Sci. Lett.*, *240*(1), 95–121, doi:10.1016/j.epsl.2005.09.041.
McLennan, S. M., et al. (2014), Elemental geochemistry of sedimentary rocks at Yellowknife Bay, Gale crater, Mars, *Science*, *343*(6169), doi:10.1126/science.1244734.
Meyers, W. J. (1974), Carbonate cement stratigraphy of the Lake Valley Formation (Mississippian) Sacramento Mountains, New Mexico, *J. Sediment. Res.*, *44*(3), 837–861.
Meyers, W. J. (1991), *Calcite Cement Stratigraphy: An Overview*, *SEPM Short Course*, vol. 25, pp. 133–148, Dallas, Tex.
Meyers, W. J., and K. C. Lohmann (1985), Isotope geochemistry of regionally extensive calcite cement zones and marine components in Mississippian limestones, New Mexico, in *Carbonate Cements*, *Soc. Econ. Pal. Min. Sp. Pub.*, vol. 36, edited by N. Schneidermann and P. M. Harris, pp. 223–239, SEPM, Tulsa, Okla.
Ming, D. W., et al. (2014), Volatile and organic compositions of sedimentary rocks in Yellowknife Bay, Gale crater, Mars, *Science*, *343*(6169), doi:10.1126/science.1245267.
Mitchener, H., and H. Torfs (1996), Erosion of mud/sand mixtures, *Coast. Eng.*, *29*(1–2), 1–25, doi:10.1016/S0378-3839(96)00002-6.
Moratto, Z., M. Broxton, R. Beyer, M. Lundy, and K. Husmann (2010), Ames Stereo Pipeline, NASA's open source automated stereogrammetry software, paper presented at 41st Lunar and Planetary Science Conference, Houston, TX, 2364.
NASA-JPL (2013), Mars Science Laboratory Project Software Interface Specification (SIS), Mast Camera (Mastcam), Mars Hand Lens Imager (MAHLI), and Mars Descent Imager (MARDI) Experiment Data Record (EDR) and Reduced Data Record (RDR) PDS Data Products, Version 1.2, JPL D-75410, SIS-SCI035-MSL, 29 October 2013. [Available at http://pdsimaging.jpl.nasa.gov/data/msl/MSLMHL_0004/DOCUMENT/MSL_MMM_EDR_RDR_DPSIS.PDF.]
O'Connor, M. P. (1972), Classification and environmental interpretation of the cryptalgal organosedimentary "molar-tooth" structure from the Late Precambrian Belt-Purcell Supergroup, *J. Geol.*, *80*(5), 592–610.
Okubo, C. H., and A. S. McEwen (2007), Fracture-controlled paleo-fluid flow in Candor Chasma, Mars, *Science*, *315*(5814), 983–985, doi:10.1126/science.1136855.
Parker, T. J., M. C. Malin, F. J. Calef, R. G. Deen, H. E. Gengl, M. P. Golombek, J. R. Hall, O. Pariser, M. Powell, and R. S. Sletten (2013), Localization and 'contextualization' of *Curiosity* in Gale crater, and other landed Mars missions, paper presented at 44th Lunar and Planetary Science Conference, Houston, Tex., 2534.
Peck, D. L., and T. Minakami (1968), The formation of columnar joints in the upper part of Kilauean lava lakes, Hawaii, *Geol. Soc. Am. Bull.*, *79*(9), 1151–1166.
Pettijohn, F. J., and P. E. Potter (1964), *Atlas and Glossary of Primary Sedimentary Structures*, 370 pp., Springer-Verlag New York, Germany.
Plummer, P. S., and V. A. Gostin (1981), Shrinkage cracks—Desiccation or synaeresis, *J. Sediment. Petrol.*, *51*(4), 1147–1156.
Pollock, M. D., L. C. Kah, and J. K. Bartley (2006), Morphology of molar-tooth structures in Precambrian carbonates: Influence of substrate rheology and implications for genesis, *J. Sediment. Res.*, *76*(2), 310–323, doi:10.2110/jsr.2006.021.
Pratt, B. R. (1998a), Molar-tooth structure in Proterozoic carbonate rocks: Origin from synsedimentary earthquakes, and implications for the nature and evolution of basins and marine sediment, *Geol. Soc. Am. Bull.*, *110*(8), 1028–1045, doi:10.1130/0016-7606(1998)110<1028:Mtsipc>2.3.Co;2.
Pratt, B. R. (1998b), Syneresis cracks: Subaqueous shrinkage in argillaceous sediments caused by earthquake-induced dewatering, *Sediment. Geol.*, *117*(1–2), 1–10, doi:10.1016/S0037-0738(98)00023-2.
Shorlin, K. A., J. R. de Bruyn, M. Graham, and S. W. Morris (2000), Development and geometry of isotropic and directional shrinkage-crack patterns, *Phys. Rev. E*, *61*(6), 6950–6957.
Siebach, K., and J. Grotzinger (2013), Volumetric estimates of ancient water on Mount Sharp based on boxwork deposits, Gale crater, Mars, *J. Geophys. Res. Planets*, *119*, 189–198, doi:10.1002/2013JE004508.
Sletten, R. S., B. Hallet, and R. C. Fletcher (2003), Resurfacing time of terrestrial surfaces by the formation and maturation of polygonal patterned ground, *J. Geophys. Res.*, *108*(E4), 8044, doi:10.1029/2002JE001914.

Smith, A. G. (1968), The origin and deformation of some "molar-tooth" structures in the Precambrian BeltPurcell Supergroup, *J. Geol.*, *76*(4), 426–443.
Stack, K. M., et al. (2014), The diagenetic origin of nodules and hollow nodules of the Sheepbed member, Yellowknife Bay formation, Gale crater, Mars, *J. Geophys. Res. Planets*, doi:10.1002/2014JE004617.
Terzaghi, K. (1944), *Theoretical Soil Mechanics*, 510 pp., John Wiley, London.
Tosca, N. J., A. H. Knoll, and S. M. McLennan (2008), Water activity and the challenge for life on early Mars, *Science*, *320*(5880), 1204–1207, doi:10.1126/science.1155432.
Tosca, N. J., F. A. Macdonald, J. V. Strauss, D. T. Johnston, and A. H. Knoll (2011), Sedimentary talc in Neoproterozoic carbonate successions, *Earth Planet Sci. Lett.*, *306*(1–2), 11–22, doi:10.1016/j.epsl.2011.03.041.
Vaniman, D., et al. (2014), Mineralogy of a mudstone at Yellowknife Bay, Gale crater, Mars, *Science*, *343*(6169), doi:10.1126/science.1243480.
Weinberger, R. (1999), Initiation and growth of cracks during desiccation of stratified muddy sediments, *J. Struct. Geol.*, *21*(4), 379–386.
White, W. A. (1961), Colloid phenomena in sedimentation of argillaceous rocks, *J. Sediment. Petrol.*, *31*(4), 560–570.
Williams, R. M., et al. (2013), Martian fluvial conglomerates at Gale crater, *Science*, *340*(6136), 1068–1072, doi:10.1126/science.1237317.
Worden, R., and S. Burley (2003), Sandstone diagenesis: The evolution of sand to stone, in *Sandstone Diagenesis: Recent and Ancient*, pp. 1–44, Blackwell Publishing Ltd., Oxford, U. K.